check for updates

ARTICLE

Comparative Study on Properties of PBAT/PBSA Film Modified by a Multi-Functional Epoxide Chain Extender or Benzoyl Peroxide

Yanfeng Zhu[1], Huidong Shi[1], Qing Ju[1], Dong Zhao[1], Yucai Shen[1,2,*] and Tingwei Wang[1,2,*]

[1]College of Materials Science and Engineering, Nanjing Tech University, Nanjing, 211816, China

[2]Suqian Advanced Materials Institute of Nanjing Tech University, Suqian, 223800, China

*Corresponding Authors: Yucai Shen. Email: ycshen@njtech.edu.cn; Tingwei Wang. Email: wangtw@njtech.edu.cn

ABSTRACT

Poly(butylene adipate-co-terephthalate) (PBAT) and poly(butylene succinate-co-adipate) (PBSA) blend films were prepared with different contents of a multifunctional epoxide chain extender Joncryl ADR-4468 (ADR) or benzoyl peroxide (BPO). The long-chain-branching (LCB) introduced by ADR and branched/crosslinked entanglement induced by BPO increased melt elasticity, viscosity and compatibility, as indicated by thermal properties, rheological and morphological analyses. It was found that the elongation at break and the tensile strength were significantly improved, due to the enhancement of compatibility and the interfacial adhesion by the incorporation of ADR or BPO. The best mechanical properties were obtained in PBAT/PBSA/ADR (60/40/0.3) (A4T6A$_{0.3}$) and PBAT/PBSA/BPO (60/40/0.9) (A4T6B$_{0.9}$) films, respectively. With the rapid initiation of chain growth by BPO, it has significantly improved the transparency of the film. ADR and BPO can be used interchangeably in improving the comprehensive properties of PBAT/PBSA films, and it would provide more strategies for developing biodegradable materials for various applications.

KEYWORDS

PBAT; PBSA; chain extend; *in-situ* compatibilization

1 Introduction

The high toughness and biodegradability of poly(butylene adipate-co-terephthalate) (PBAT) have made it one of the primary materials used to replace traditional plastics in disposable products, flexible packaging, agricultural films and other fields [1]. Current methods for modifying PBAT thin films fall into four categories. The first approach is based on blending PBAT with traditional plastics, such as polypropylene (PP) and polyethylene (PE) [2,3]. The second category consists of blends of PBAT with degradable polyesters, such as poly(lactic acid) (PLA), poly(butylene succinate) PBS, and poly(propylene carbonate) PPC [3–5]. The third approach blends PBAT with inorganic fillers such as adding silane coupling agents, and compatibilizers [6,7]. The final category of modification methods is based on blending PBAT with biomass-based materials such as lignin, starch and natural fiber reinforcements [8,9]. Among these modification methods, blending and reactive compatibilization of PBAT with biodegradable polyesters is the most common, and blends of PBAT and PLA are highly studied and have been utilized in a broad range of commercialized applications. However, given the inherent limitations of the neat materials, significant

efforts are still needed to improve the poor compatibility between PBAT and PLA. Moreover, the high processing temperatures required for PLA cause thermal degradation of PBAT. With these challenges in mind, PBSA appears to be an excellent substitute for PLA. The aliphatic chain structures of PBSA and PBAT are similar, thus PBSA partially mixes with PBAT. Both polymers also have similar glass transition temperatures and melting points [10], which not only reduces the necessary processing temperature, but also makes the blend more fluid during processing. Moreover, like PLA, which is commonly blended with PBAT, the high strength and modulus of PBSA should improve the strength and stiffness of the resulting blends.

Presently, several groups have developed biodegradable polymer blends with outstanding processing abilities and mechanical properties thanks to the complementary properties of each component [11–13]. In general, improving the compatibility between the polymer components is key to multi-phase blending modification of these materials [14], as most biodegradable polyesters easily degrade during processing [15]. To minimize these drawbacks, several researchers have devoted significant efforts to the development of thermally-stable compatibilizers for multi-biodegradable polymers. Some of these efforts include the use of chain extenders containing multi-reactive compounds that are able to react with the carboxyl or hydroxyl groups in the polymer fragments generated during processing. Kopinke et al. [16] used a chain extender introducing the long branched structures to alleviate the thermal degradation of PLA during melting. Such chain extenders include di-isocyanate compounds [17], bisoxazolines [18] and multifunctional epoxide compounds [19]. However, the toxicity and volatility of isocyanate compounds and bisoxazolines make them harmful to people, which limits their application in environmentally friendly packaging.

Epoxy-containing multifunctional chain extenders also have been used in biodegradable polymers. Najafi et al. [20] compared the effects of tris(nonyl-phenyl) phosphate (TNPP), polycarbodiimide (PCDI) and a multifunctional epoxide chain extenders on the thermal stability of PLA. Since the epoxy-based compounds react with both types of end groups (-OH and -COOH) on the polymers, these chain extenders form a large number of branches and improve the interfacial adhesion and compatibility of the two phases [21]. Another well-studied chain extension strategy is the use of peroxides, as the peroxides act as free-radical initiators for the in situ compatibilization of polymers. Yan et al. [22] prepared PBS/waxy starch blends using benzoyl peroxide (BPO) as a crosslinking agent. BPO could act as a free radical initiator for the *in-situ* compatibilization of PBAT/PBSA blends, and its compatibilization effect is different from ADR.

Inspired by these approaches that use reactive compounds to improve the compatibility between polymers, the goals and motivation of this work were to study the effects of ADR and BPO, a chain extender and free radical initiator, respectively, on the properties of PBAT/PBSA blends. Both ADR and BPO change the mechanical and rheological properties of polymer blends by promoting the continuous growth, branching and even cross-linking of the molecular chains [23,24]. Scheme 1 shows the reaction mechanism of PBAT/PBSA with ADR or BPO. Accordingly, it is worth investigating if ADR and BPO can be used interchangeably without adversely affecting the performance of the resulting PBAT/PBSA blends. Since the characteristic temperatures of PBAT and PBSA are similar, the molecular structures formed after chain extension and branching are more complex. There may be different optimal conditions for the two additives to achieve the best miscibility and comprehensive performance in the blends. Therefore, the effects of different amounts of the ADR additive on the rheological, mechanical, and thermodynamic properties as well as the morphology of PBAT/PBSA blends were compared with blends prepared with BPO in this work.

(a)   The reaction formula of ADR

(b)   The reaction formula of BPO
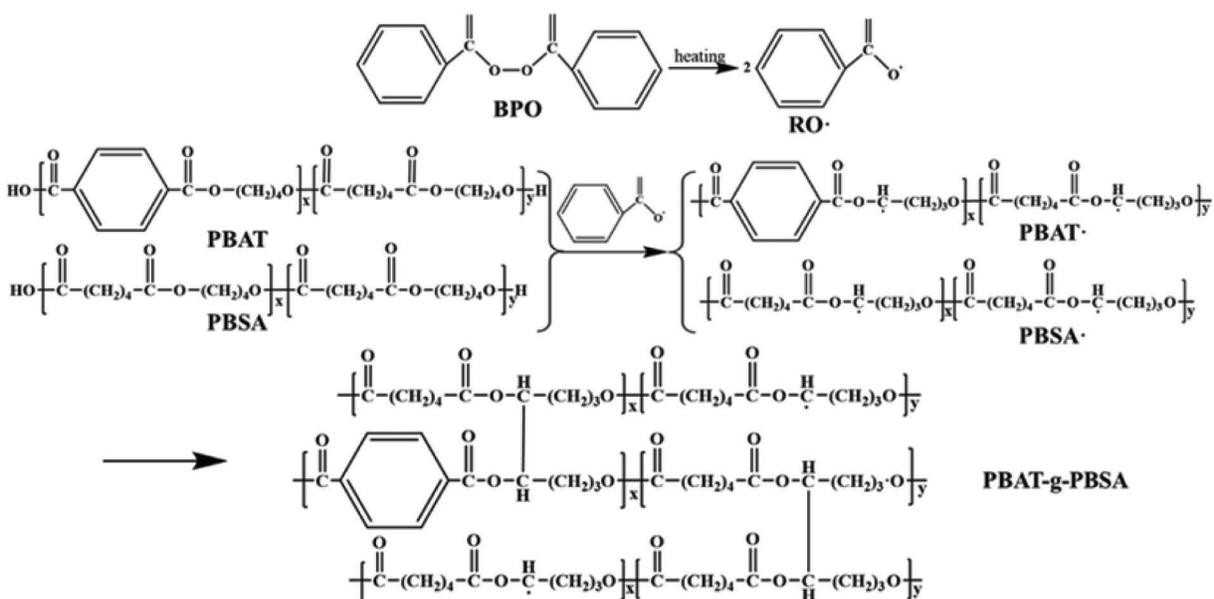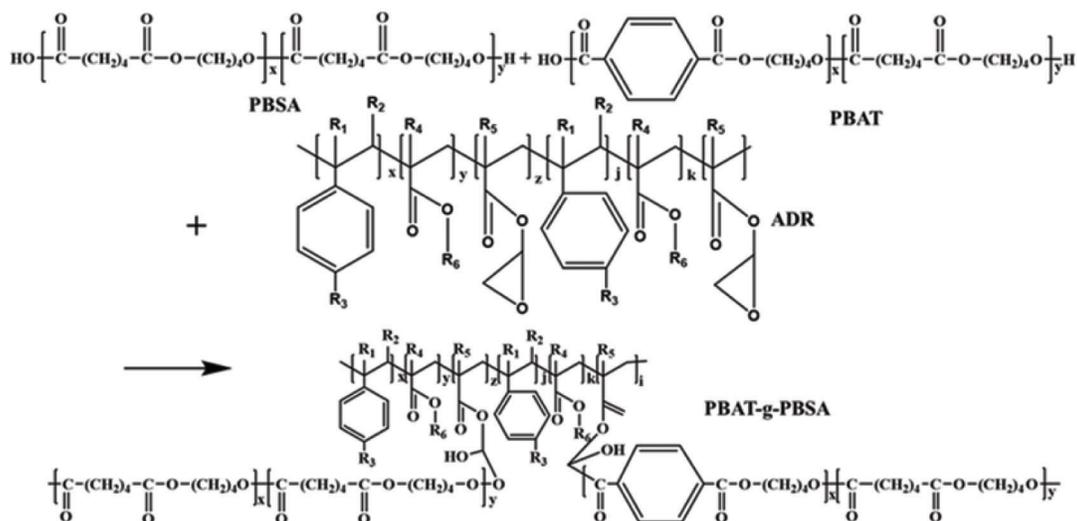
Scheme 1: The reaction mechanism of (a) ADR and (b) BPO

2 Experiment

2.1 Materials

Poly(butylene adipate-co-terephthalate) (PBAT Biocosafe2003) was obtained from Hangzhou Xinfu Technology Co., Ltd. (China), with an average molecular weight (Mw) of 5.32×10^4. Poly(butylene succinate-co-adipate) (PBSA TH801T) was supplied by Xinjiang Blue Ridge Tunhe Sci. & Tech. Co., Ltd. (China), with an average molecular weight (Mw) of 1.53×10^5. A styrene-acrylic multi-functional epoxide oligomeric agent (Joncryl ADR-4468) was purchased from BASF, with the molecular weight of 6800 g/mol and containing 5~10 epoxy groups per molecule. Benzoyl peroxide (BPO) was provided by

Shanghai Tianlian Fine Chemical Co., Ltd. (China). Tetrahydrofuran (THF) was purchased from Shanghai Shisihewei Chemical Co., Ltd. (China). BPO and THF were reagent grade and used without further purification.

2.2 Sample Preparation

2.2.1 Melt Blending of Samples

PBAT and PBSA were dried at 60°C in a vacuum drying oven before blending. Polymer blends were manually mixed and then added into an internal mixer of XSS-300 torque rheometer, which was controlled steadily at a temperature of 130°C and rotation speed of 60 rpm. After mixing for 5 min, required amount of ADR or BPO was added to the mixer, and continued for 5 min. The formulations are presented in Table 1.

Table 1: The composition of samples

Samples	PBAT (wt%)	PBSA (wt%)	ADR (wt%)	BPO (wt%)
A4T6	60	40	0	0
A4T6A$_{0.1}$	60	40	0.1	0
A4T6A$_{0.3}$	60	40	0.3	0
A4T6A$_{0.6}$	60	40	0.6	0
A4T6A$_{0.9}$	60	40	0.9	0
A4T6A$_{1.2}$	60	40	1.2	0
A4T6B$_{0.1}$	60	40	0	0.1
A4T6B$_{0.3}$	60	40	0	0.3
A4T6B$_{0.6}$	60	40	0	0.6
A4T6B$_{0.9}$	60	40	0	0.9
A4T6B$_{1.2}$	60	40	0	1.2

2.2.2 Processing of Films

The films were prepared by hot pressing for 3 min at a temperature of 140°C with a pressure of 10 MPa. Then, cold pressing was applied with a pressure of 10 MPa. The dimensions of films were 150 mm × 130 mm × 0.2 mm and 150 mm × 130 mm × 0.5 mm for follow-up characterization and testing.

2.3 Methods

The melt flow index (MFI) of the samples were measured using a melting index instrument (Dongguan Dongri Instrument Co., Ltd. (China) DR-801) in accordance with ASTM D1238-2010. The temperature of the melt was kept at 190°C with a 2.16 kg load.

Thermal properties of the films were measured using a differential scanning calorimeter (DSC204 F1 Phoenix) under a nitrogen atmosphere. All samples were heated from 25°C to 160°C at a rate of 10 °C/min and held at 160°C for 1 min to erase the thermal history, then they were cooled to −60°C at 10 °C/min and reheated under the same conditions. The crystallization temperature (T_c), melting temperature (T_m), and the enthalpy of melting and cold crystallization (ΔH_m and ΔH_{cc}, respectively) of the samples were obtained from the DSC thermograms.

The dynamic rheological behavior of the film was tested by a dynamic rheometer (DHR-18 TA Instruments USA) at 160°C. Small amplitude oscillatory shear frequency sweeps were carried out in the

linear viscoelastic region at frequency of 0.1 to 100 rad/s with 1% strain for all samples. The sample size was 25 mm in diameter and 0.5 mm in thickness. Prior to testing, the sample was held at 160°C for 2 min to erase its thermal history.

The dynamic mechanical thermal analysis was also investigated by a dynamic rheometer (DHR-18 TA Instruments USA). A dual cantilever clamp was used at a frequency of 1 Hz. The samples were heated from −80°C to 40°C at a heating rate of 3 °C/min. The sample size was 40 mm × 5 mm × 0.5 mm. The storage modulus (E′), loss modulus (E″) and loss factor (tan δ) of the sample were obtained with temperature.

The mechanical properties of the films were determined using a computer control electronic universal testing machine (CMT5254 Shenzhen Sans Measurement Technology Co., Ltd., China) in accordance with ASTM D882-2018. The dumbbell-shaped specimens (25 mm × 4 mm × 0.2 mm) were conditioned for 24 h in a desiccator at 25°C and 50% relative humidity. The tested temperature was 25°C and cross head speed was 200 mm/min. The average of five measured values was reported for each formulation.

Film light transmittance test was conducted by a photoelectric haze meter (WGW Shanghai Precision Scientific Instrument Co., Ltd., China) in accordance with ASTM D1003-61-1997. 50 mm × 50 mm × 0.2 mm square film was cut from the film and tested at room temperature.

Themorphology of films was analyzed by a scanning electron microscope (JSM-650 JEOL Japan). The samples were immersed in liquid nitrogen to break and then coated with a thin layer of gold to enhance the conductivity before observation. In order to further observe the polymer phase of the blend, the surface of the film was etched with tetrahydrofuran (THF) for 10 min. THF solvent is able to selectively dissolve PBAT. All samples were dry before observation.

3 Results and Discussion

3.1 Melt Flow Properties

The flow behavior of a polymer blend melt greatly influences its preparation and processing conditions. The flow properties at high temperatures can be measured by MFI and reflect the molecular weight, molecular weight distribution and degree of cross-linking in the blend [25]. Fig. 1a shows the MFI results of neat PBAT and PBSA without and with added ADR and BPO. It can be seen that the PBSA melt was highly fluid, suggesting that blending PBSA with PBAT should improve the processing fluidity of PBAT [26]. The MFI results also showed that the two additives led to some chain extension and branching in both PBAT and PBSA. In particular, the MFI values decreased significantly after adding ADR and BPO to the highly fluid PBSA melt. The MFI values of PBAT/PBSA/ADR and PBAT/PBSA/BPO blends decreased with increasing ADR and BPO contents, as shown in Fig. 1b. As a chain extender, ADR could increase the molecular weight of PBAT and PBSA through the ring opening reaction of epoxy groups, while BPO can induce the crosslinking of the blend system. Comparing the effects of ADR and BPO in A4T6 suggested that the initiator BPO had a better tackifying effect. The results showed that the melt flow properties of the matrix could be tuned from high to low by changing the chain extender content, thus adapting to different processing and forming methods such as extrusion, blow molding, film blowing and foaming [27].

3.2 Thermal Properties

The first cooling and second heating curves from DSC measurements of the films are shown in Fig. 2, and the relevant data is summarized in Table 2. ADR and BPO had little effect on the T_m of the blends. As the content of the two additives increased, the T_g values increased slightly, and the subsequent DMTA analysis is discussed in more detail below. The DSC data for the PBSA/PBAT (A4T6) film showed two crystallization peaks, which corresponded to the crystallization of PBSA at the higher temperature followed by PBAT at the lower temperature.
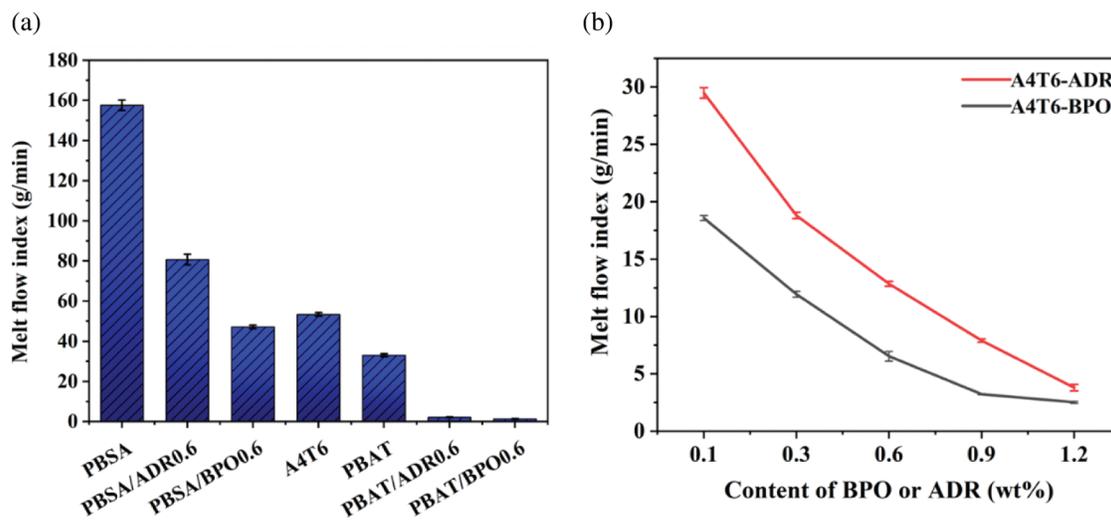
(a)

(b)

Figure 1: Melt flow index of (a) different composition and (b) A4T6 with ADR or BPO
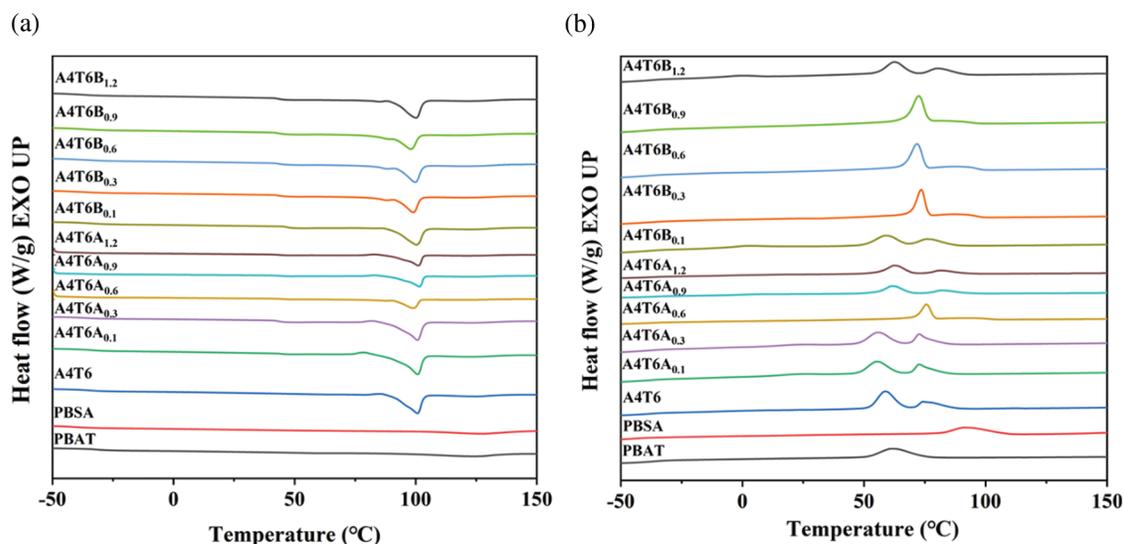
(a)

(b)

Figure 2: DSC curves of samples from (a) the second heating and (b) the first cooling

Upon addition of 0.1 wt% and 0.3 wt% ADR, it was found that the crystallization peaks moved to lower temperatures as shown in Fig. 2b. Note that in these samples, the two peaks in the blends did not simply correspond to the crystallization peaks of the two neat polymer components because the crystallization temperature ranges of PBAT and PBSA overlapped [28]. The data also showed that a few weight percent of ADR promoted crystallization in the blends. A single main peak was observed for the blend prepared with 0.6 wt% ADR as well as the blends containing BPO. As was previously discussed with regards to the MFI results, the chain extension reaction not only occurred between either PBAT and PBSA, but also reacted with both components to form PBAT-g-PBSA [29], thereby improving the compatibility of the blends.

Table 2: DSC parameters for samples, where T_{c1} is smaller peak and T_{c2} is larger peak from the first cooling curves

Sample	T_g (°C)	T_{c1} (°C)	T_{c2} (°C)	ΔH_{cc} (J/g)	T_m (°C)	ΔH_m (J/g)
PBAT	−32.1	58.5	/	13.5	122.9	17.4
PBSA	−36.8	91.9	/	26.4	127.4	38.5
A4T6	−34.7	58.6	74.3	27.6	100.7	33.6
A4T6A$_{0.1}$	−33.6	55.1	72.7	25.4	100.5	35.5
A4T6A$_{0.3}$	−33.6	55.6	72.7	24.8	100.5	34.6
A4T6A$_{0.6}$	−34.2	75.5	75.5	22.3	99.5	28.7
A4T6A$_{0.9}$	−34.2	61.4	82.2	23.7	101.2	29.8
A4T6A$_{1.2}$	−33.5	62.3	81.7	25.3	101.2	30.5
A4T6B$_{0.1}$	−34.5	58.7	76.9	20.6	99.8	30.6
A4T6B$_{0.3}$	−33.4	73.4	73.4	21.6	98.7	24.4
A4T6B$_{0.6}$	−33.3	71.7	71.7	20.3	98.7	26.4
A4T6B$_{0.9}$	−33.3	72.4	72.4	22.1	98.3	24.9
A4T6B$_{1.2}$	−34.9	62.3	80.0	20.9	99.8	24.5

That DSC data showed a single peak at lower BPO weight fractions, suggesting that heterogeneous nucleation of PBAT induced PBSA crystallization and the *in-situ* compatibilization effects of crosslinked graft copolymer produced with BPO were more obvious [30]. As the BPO content increased, the main peak shifted to lower temperatures, and the fluctuations in the slope were more obvious. As the additive content further increased, the DSC data for the blends again showed two distinct peaks at low temperatures. These results suggest that a critical amount of the ADR and BPO additives were needed, which corresponded to the blends prepared with the lowest additive mass fraction that showed a single crystal peak in the DSC data. As the amount of additive in the blend continued to increase, the molecular chain lengths continued to grow, and the degree of branching or even crosslinking further increased, which increased the probability of the formation of longer chains. These more complex molecular chain architectures also had distinct melting temperatures. Therefore, two distinct peaks were seen in the DSC data for higher ADR and BPO amounts, but at higher temperatures than for the blends prepared with little or no additive. As more additive was incorporated into the blend, the molecular weight of the chains increased, and the increased number of long branches and cross-linked points acted as nucleation sites [31], which shifted the two crystallization peaks to higher temperatures.

3.3 Rheological Properties

Figs. 3a–3f show results of dynamic complex viscosity (η^*), storage modulus (G'), and loss modulus (G''). As shown in Figs. 3a and 3b, compared with the pure matrix, the complex viscosity of all the blends increased significantly. Neglecting potential effects of thermal degradation of the polymers during the tests [32], the degree of shear thinning increased as the additive content increased. Even so, the complex viscosity of the blends prepared with small amounts of the additives was three times higher than that of the neat polymer matrix. In addition, the slopes of the viscosity curves measured for the ADR-modified polymer blends did not change significantly with ADR content, while the BPO-modified blends showed more shear thinning behavior at high BPO contents. The higher viscosity at low sweep frequencies of BPO-based blends reflected the higher degree of molecular branching or crosslinking [33]. At high frequency, the stronger shear thinning illustrated that the crosslinking and network were more

likely formed under the action of BPO. Unlike with ADR, initiation of the chain extension with BPO was not confined to the chain ends, and dehydrogenation could occur along the chain backbone, which made the formation of macromolecular chain entanglements easier [34,35]. However, these macromolecular chain entanglements would be disentangled significantly at high sweep frequencies, thus the complex viscosity eventually plateaued to a stable value that was not significantly different from the complex viscosity measured for the ADR-based blends.
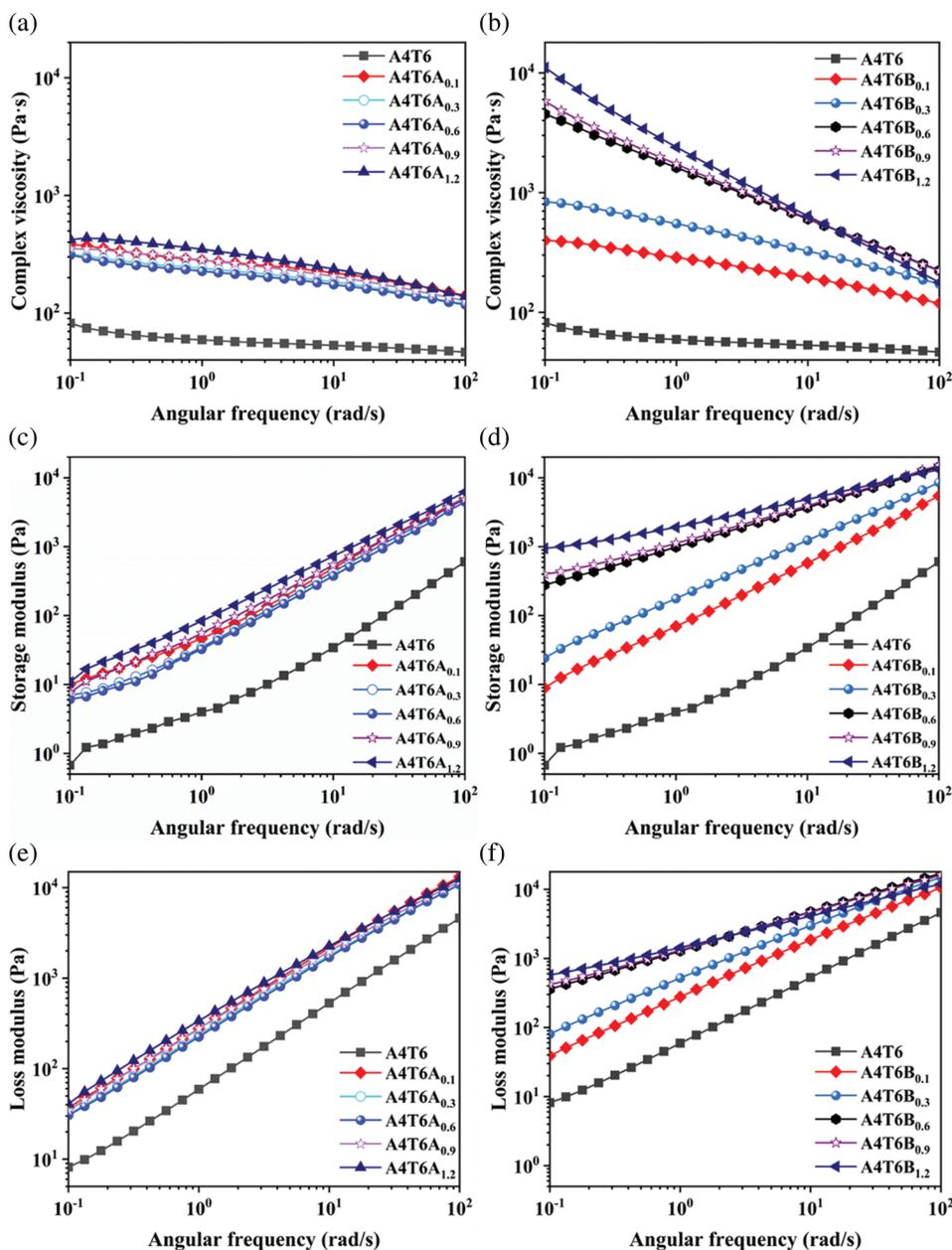

Figure 3: (a–b) Complex Viscosity (η^*), (c–d) storage modulus (G') and (e–f) loss modulus (G'') curves of all samples

The storage modulus (G′) and loss modulus (G″) provided more insights into the molecular chain extension and branching phenomena in the blends. As shown in Figs. 3c and 3d, the storage modulus increased significantly as the ADR and BPO content increased, indicating that the two additives improved the melt strength of the blends [36]. Since simple star and linear polymer structures do not lead to a significant increase in the structural elasticity of melts [37], the long-branched chain structures formed by the BPO-initiated reactions likely entangled more easily and formed physical entanglement points [38]. In Figs. 3e and 3f, blends containing a small amount of BPO showed a loss modulus comparable to blends prepared with ADR at low frequencies, but the measured loss moduli for both types of blends converged to the same value at high frequencies. Because the polymeric molecular segments do not have enough time to relax in the high-frequency region, the material stores more energy. ADR acting as chain extender increases the molar mass of the polymer chains at the interface and improved the interface adhesion, therefore, the chain segment relaxation time increases and the energy loss also increases at low frequency. Unlike ADR, with the increase of BPO content, the G′ and G″ increased significantly at low frequency. Because the interaction and entanglement between the two phases are enhanced with the aid of BPO, the melt of the blend can absorb more energy under deformation, therefore, the blend has greater viscoelasticity. Further combined with the G′ results, although the G′ curves had no obvious intersection points with the G″ curves, as the additive content increased, the two curves approached one another. These results showed that ADR enables as many molecules as possible to grow into long-chain-branching (LCB) structure, however, BPO promotes the formation of branched/crosslinked network due to efficient free radical reaction. A diagram of the ADR and BPO chain extension mechanisms based on the DSC and rheology results is shown in Scheme 2.
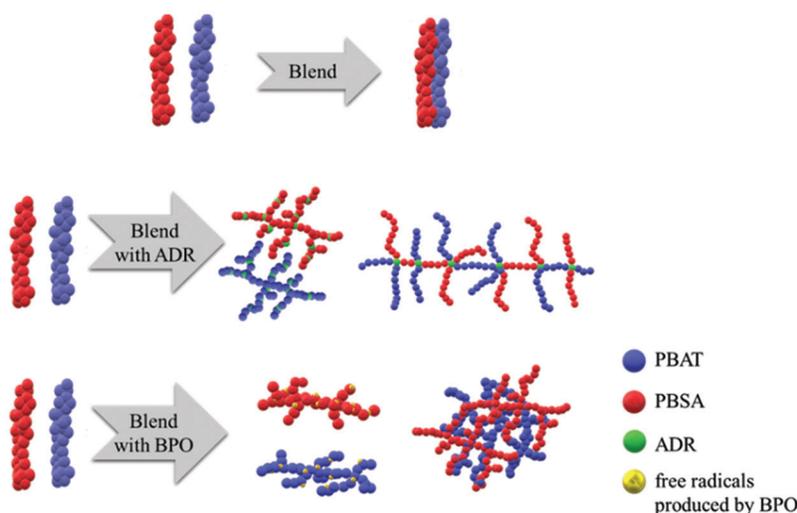
Scheme 2: Chain extension mechanism model of ADR and BPO

3.4 Dynamic Mechanical Thermal Properties

Dynamic mechanical thermal analysis (DMTA) was used to evaluate the influence of ADR and BPO on the compatibility of the blend components. Figs. 4a–4d show the curves of storage modulus (E′) and loss factor (tan δ). The DMTA parameters are listed in Table 3. As seen in Figs. 6a and 6b, E′ measured for all prepared blends decreased with an increase in temperature, which corresponded to the relaxation process due to polymer flow. Consistent with the trends in tan δ, the curves did not have the shape characteristic of two-phases, and the sudden drop in value represented the T_g of the blends. After adding BPO, the storage modulus of the blends at 25°C decreased due to the increase in amorphous area. As

shown in the DSC results discussed above, BPO addition reduced the ΔH_m of the blends, indicating that the overall crystallinity of the blend was reduced [39]. The factors that affect the thermodynamic properties of polymer phase transitions are chemical bonds, van der Waals forces, hydrogen bonds, and compatibility of the components [40]. Regarding the PBAT/PBSA blends, the enthalpy of the phase transition was mainly determined by the intermolecular forces and compatibility of the two phases. The rigid group introduced by ADR had a small effect on the strength of the blends and improved the E′ at 25°C slightly.
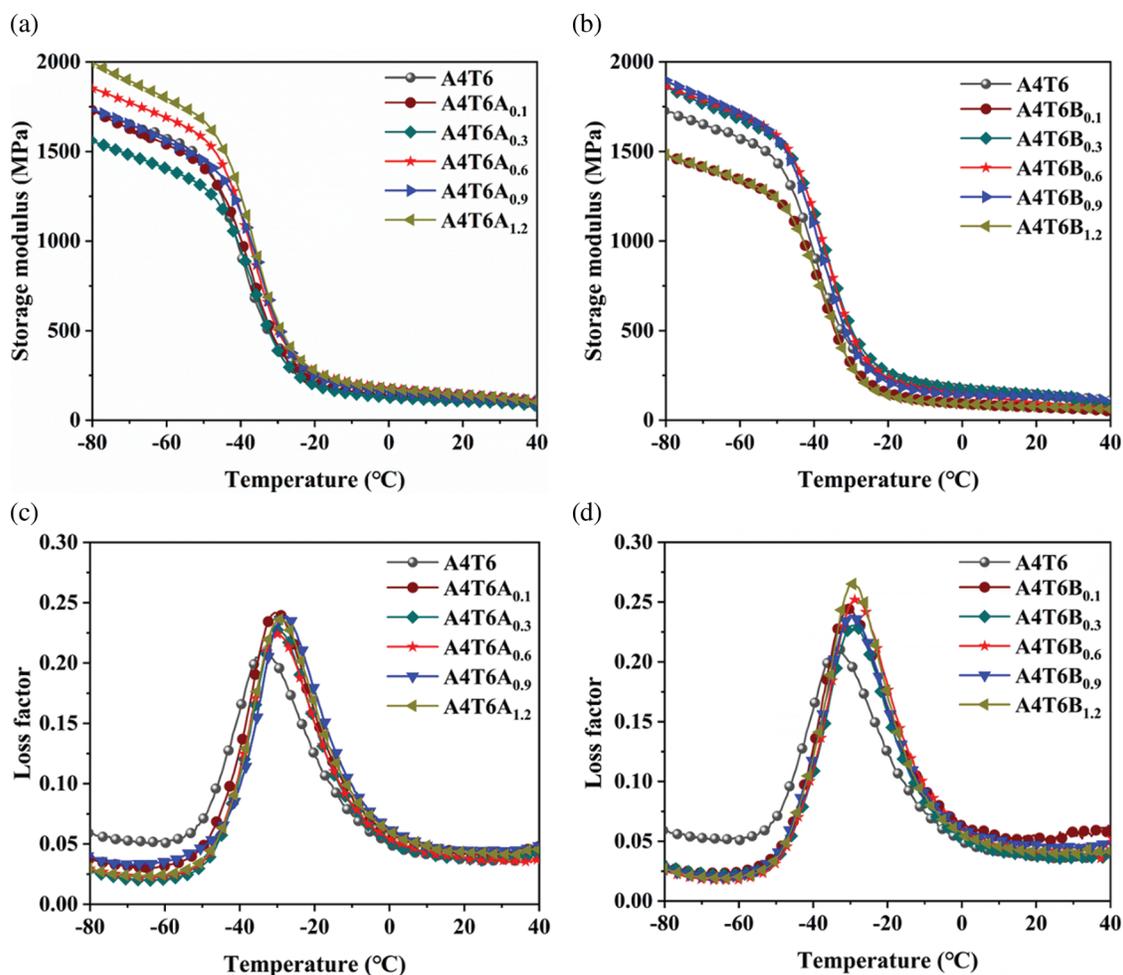

Figure 4: (a–b) Storage modulus (E′) and (c–d) loss factor (tan δ) curves of all samples

Figs. 4c and 4d showed tan δ *vs.* the temperature of the blends. Here tan δ was used to determine the T_g values of the blends shown in Table 3. All samples presented only one relaxation peak, corresponding to the T_g of blends. The shift of the peak showed that T_g increased within a small range, which was consistent with the DSC results. The higher peak values of tan δ also illustrated that the reactions between the PBAT and PBSA chains initiated with both ADR and BPO enhanced the interfacial interactions in the blends. As in the rheological analysis, the DMTA results suggested that the branches and crosslinks hindered the movement of the macromolecular segments, but the graft copolymer PBAT-g-PBSA at the two-phase interface further compatibilized the blends.

Table 3: DMTA parameters for samples

Samples	T_g (°C)	E′ at 25°C (MPa)
PBAT	−27.4	53.2
A4T6	−30.4	108.2
A4T6A$_{0.1}$	−30.7	114.2
A4T6A$_{0.3}$	−30	105.1
A4T6A$_{0.6}$	−27.1	139
A4T6A$_{0.9}$	−28.3	124.4
A4T6A$_{1.2}$	−28.9	135.8
A4T6B$_{0.1}$	−30.4	70.2
A4T6B$_{0.3}$	−28.8	139.3
A4T6B$_{0.6}$	−28.3	90.8
A4T6B$_{0.9}$	−27.3	101.4
A4T6B$_{1.2}$	−28.9	75.1

3.5 Mechanical Properties

As shown in Fig. 5, pure PBAT had a high toughness, low strength and low modulus. Meanwhile, PBSA had high tensile strength, high elastic modulus, and low elongation at break and complemented the mechanical limitations of PBAT [41]. In our basic experiment of PBAT/PBSA blend with different proportions, we found that A4T6 component film not only maintained the high toughness of PBAT, but also had good tensile strength. However, the addition of high content of PBSA reduces the compatibility and has a negative impact on the mechanical properties. After the blend system was compatibilized by ADR and BPO, the mechanical properties of the films were improved. As shown in Fig. 6, the best mechanical properties were obtained in blends of these polymers prepared with 0.3 wt% ADR and 0.9 wt% BPO, respectively. When 0.3 wt% ADR was added to the blend, the tensile strength and elongation at break of the film were 23.2 MPa and 923%, respectively, and when the content of BPO was 0.9 wt%, the tensile strength and elongation at break were 24.2 MPa and 894%, respectively. As the content of the two additives increased, the tensile strength and elongation at break first increased and then decreased, reflecting the negative impact of incomplete or excessive chain extension on the mechanical properties of the blends. As mentioned in the DMTA analysis, the strength and toughness of the films were greatly affected by the intermolecular forces and two-phase compatibility. When an appropriate amount of ADR or BPO was added, the branched entanglements formed by the extended molecular chains improved the strength of the films. The branched copolymers generated by the chain extension reactions improved the compatibility between the phases and toughened the whole matrix such that the tensile strength and elongation at break improved. In summary, the best performance in terms of the elongation at break and tensile strength was achieved by adding 0.3 wt% ADR to the PBAT/PBSA blends, as ADR addition introduced rigid benzene rings into the blend, promoted chain branching and improved the *in-situ* compatibilization between phases. In contrast, the extent of macromolecular crosslinking, increased amorphous phase content and improved *in-situ* compatibilization contributed to the optimal performance of blends prepared using 0.9 wt% BPO.
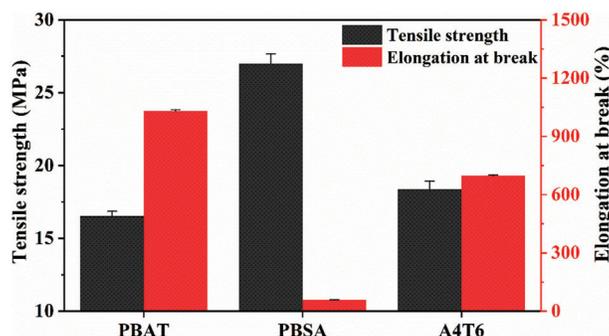
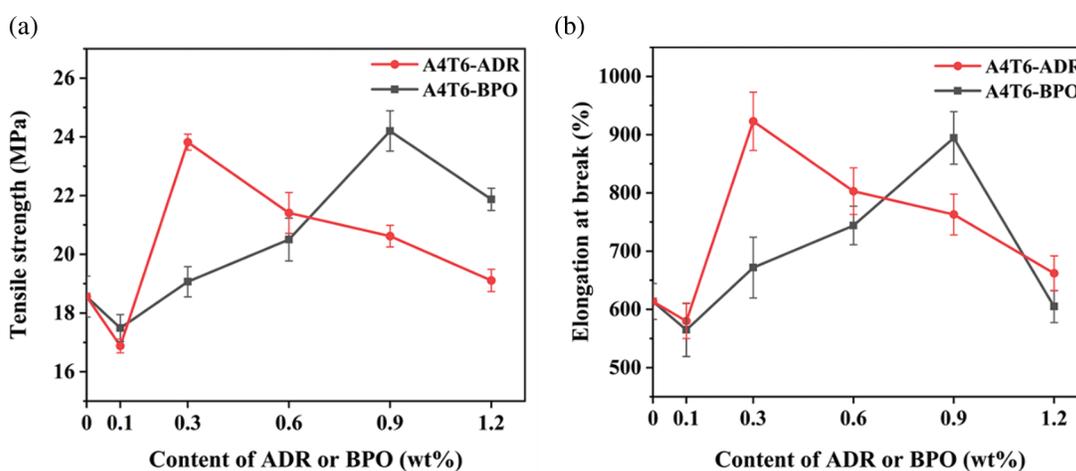**Figure 5:** Mechanical properties of PBAT, PBSA and unmodified PBAT/PBSA

Figure 6: (a) Tensile strength and (b) elongation at break of A4T6 with ADR or BPO

3.6 Optical Properties

The light transmittance of the film is shown in Figs. 7a and 7b. The results showed that the addition of PBSA reduced the light transmittance of the blend film, but the light transmittance was improved to some extent after adding ADR and BPO. This was attributable to the addition of the two additives improved the matrix compatibility and increased the interfacial bonding. Figs. 7A–7C show the apparent transparency of the film. The slight increase of $A4T6A_{0.6}$ transparency was due to the smaller size of the dispersed phase, which is the consequence of the interfacial compatibilization between PBAT and PBSA phases. Obviously, $A4T6B_{0.6}$ film showed high visible light transparency. It reflected that BPO had a better in-situ compatibilization effect than ADR.

3.7 Micromorphology

Scanning electron microscopy photographs of the quenched section of films are given in Figs. 8A–8I. The cross section of A4T6 was relatively flat in Fig. 8A, but there were a few elliptical microscopic regions. These elliptical regions were observed at higher magnifications as shown by the red arrow in Fig. 8A. It was found that PBSA had a few isolated regions in the PBAT matrix, and PBSA dispersed particles could be clearly observed, which did not appear in other components. Matos Costa et al. [42] observed similar phenomenon in PBAT/PBS (70/25). Under the action of 0.3% ADR, a small amount of ADR significantly improved the dispersion of PBSA, and the section presented a flat and smooth rigid section, as shown in Fig. 8B. At this time, the film has good toughness and strength. However, the reactive

compatibilization effect of BPO was stronger, which significantly changed the section shape, and its best mechanical properties appeared in the component containing 0.9 wt% BPO. In Fig. 8H, the section reduces the stepped ductile texture and increases the rigid fracture platform. Excessive BPO aggravated the crosslinking entanglement of the system and might have a negative impact on the mechanical properties. Obviously, the *in-situ* compatibilization effect produced by ADR or BPO greatly improved two-phase compatibility. For films modified by BPO, the fracture surfaces became rougher than that of ADR, demonstrating better interfacial adhesion.
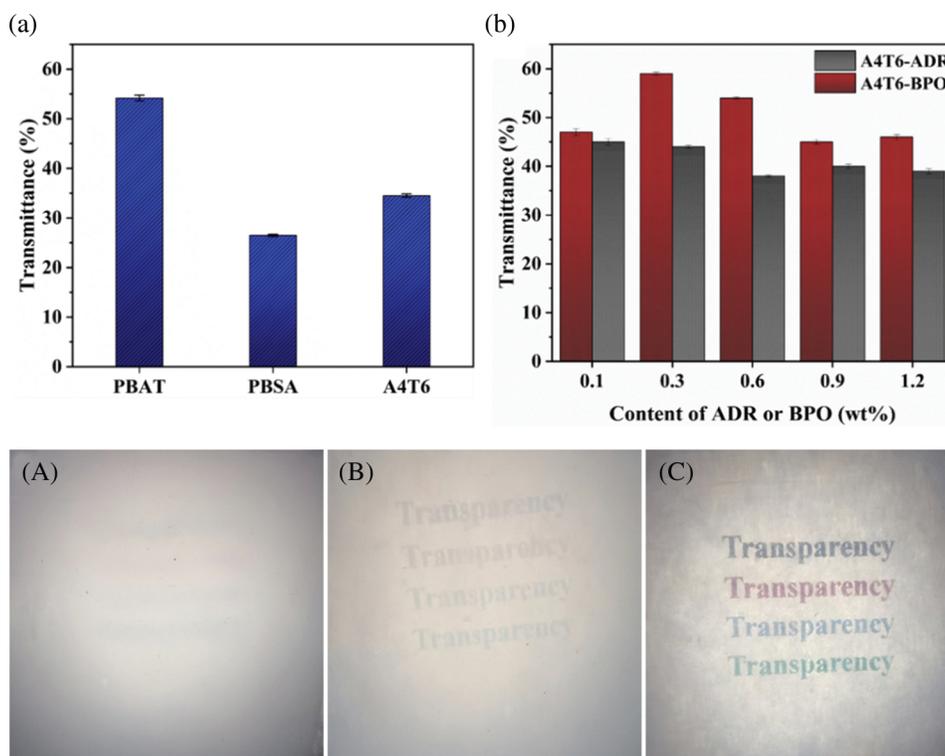

Figure 7: Transmittance of (a) PBAT, PBSA, A4T6 and (b) A4T6 with ADR and BPO; Apparent transparency of (A) A4T6, (B) A4T6A$_{0.6}$ and (C) A4T6B$_{0.6}$

The etched surfaces of films were shown in Figs. 8J–8L in order to better understand the structure and morphology of the two phases. The etched polymer phase was mainly PBAT. The film containing ADR had larger pore density and smaller pore diameter compared with unmodified film. There were no obvious etching holes presented in Fig. 8L, which may result from the better compatibility by BPO due to the formation of branched entanglement of macromolecules.
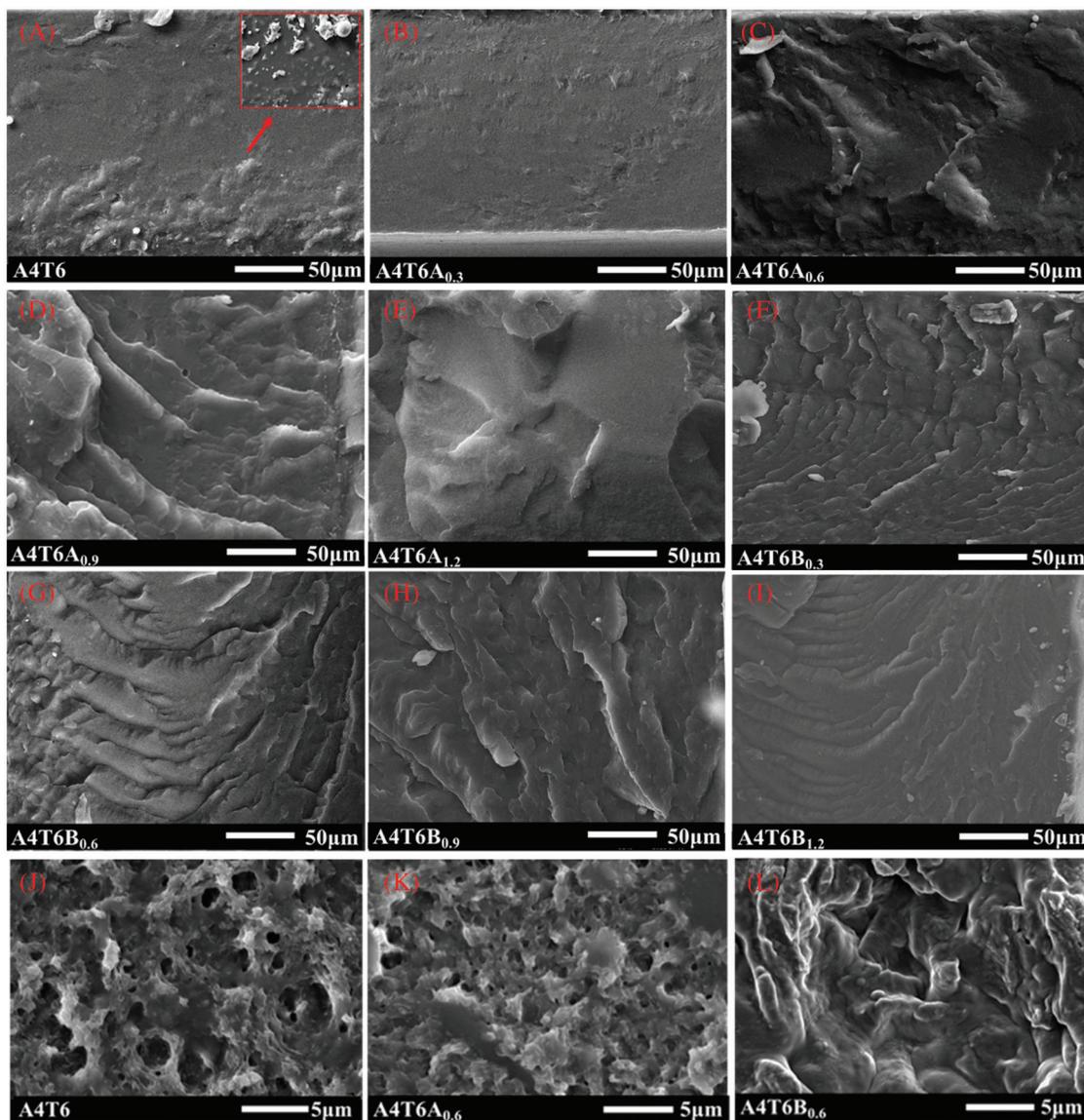
Figure 8: SEM images of (A–I) film section with quenched and (J–L) film surface with etched

4 Conclusions

Both the chain extender ADR and the initiator BPO can be used as in-situ compatibilizer to modify the PBAT/PBSA blend. ADR enables as many molecular chains as possible to grow into long-chain-branching structure, while BPO promotes the formation of branched or crosslinked structure due to efficient free radical reaction. There was a single-double peak change on the DSC curve, which corresponded to the degree of reaction and the main conversion involved in the reaction, depending on the content of the two additives. The rheological analysis results showed that ADR and BPO increased the complex viscosity and melt strength of blends. The tan δ curve illustrated the addition of BPO and ADR greatly improved the compatibility of the system, but BPO had a better compatibilization effect.

With the increase of the content of the two additives, the PBAT-g-PBSA generated by the reaction played an *in-situ* compatibilization role, and improved the interfacial bonding between the two phases. As

a result, the elongation at break and tensile strength of the blends containing 0.3 wt% ADR or 0.9 wt% BPO reached the maximum values. The light transmittance of the film increased from 34.8% to 59.7% under the action of BPO, which was much better than that of ADR. These similarities and differences between ADR and BPO on A4T6 films would provide more strategies for the development of biodegradable films in various applications.

Conflicts of Interest: The authors declare that they have no conflicts of interest to report regarding the present study.

References

1. Serrano-Ruiz, H., Martin-Closas, L., Pelacho, A. M. (2021). Biodegradable plastic mulches, impact on the agricultural biotic environment. *Science of the Total Environment, 750,* 141228. DOI 10.1016/j.scitotenv.2020.141228.

2. Behera, K., Veluri, S., Chang, Y., Yadav, M., Chiu, F. (2020). Nanofillers-induced modifications in microstructure and properties of PBAT/PP blend, enhanced rigidity, heat resistance, and electrical conductivity. *Polymer, 203,* 122758. DOI 10.1016/j.polymer.2020.122758.

3. Bumbudsanpharoke, N., Wongphan, P., Promhuad, K., Leelaphiwat, P., Harnkarnsujarit, N. (2022). Morphology and permeability of bio-based poly(butylene adipate-co-terephthalate) (PBAT), poly(butylene succinate) (PBS) and linear low-density polyethylene (LLDPE) blend films control shelf-life of packaged bread. *Food Control, 132,* 108541. DOI 10.1016/j.foodcont.2021.108541.

4. Nofar, M., Salehiyan, R., Ciftci, U., Jalali, A., Durmuş, A. (2020). Ductility improvements of PLA-based binary and ternary blends with controlled morphology using PBAT, PBSA, and nanoclay. *Composites Part B: Engineering, 182,* 107661. DOI 10.1016/j.compositesb.2019.107661.

5. Jiang, G., Li, H. F., Wang, F. (2021). Structure of PBAT/PPC blends prepared by *in-situ* reactive compatibilization and properties of their blowing films. *Materials Today Communications, 27,* 102215. DOI 10.1016/j.mtcomm.2021.102215.

6. Jian, J., Zeng, X. B., Huang, X. B. (2020). An overview on synthesis, properties and applications of poly(butylene-adipate-co-terephthalate)-PBAT. *Advanced Industrial and Engineering Polymer Research, 3(1),* 19–26. DOI 10.1016/j.aiepr.2020.01.001.

7. Xu, Y. F., Huang, C. X., Dang, X., Khan, M. R., Huang, H. et al. (2020). Preparation of long-term antibacterial SiO_2-cinnamaldehyde microcapsule via Sol-gel approach as a functional additive for PBAT film. *Processes, 8(8),* 897. DOI 10.3390/pr8080897.

8. Fourati, Y., Tarres, Q., Delgado-Aguilar, M., Mutje, P., Boufi, S. (2021). Cellulose nanofibrils reinforced PBAT/TPS blends: Mechanical and rheological properties. *International Journal of Biological Macromolecules, 183,* 267–275. DOI 10.1016/j.ijbiomac.2021.04.102.

9. Liu, Y. F., Liu, S., Liu, Z. T., Lei, Y., Jiang, S. Y. et al. (2021). Enhanced mechanical and biodegradable properties of PBAT/lignin composites via silane grafting and reactive extrusion. *Composites Part B: Engineering, 220,* 108980. DOI 10.1016/j.compositesb.2021.108980.

10. Nofar, M., Oguz, H., Ovalı, D. (2019). Effects of the matrix crystallinity, dispersed phase, and processing type on the morphological, thermal, and mechanical properties of polylactide-based binary blends with poly[(butylene adipate)-co-terephthalate] and poly[(butylene succinate)-co-adipate]. *Journal of Applied Polymer Science, 136(23),* 47636. DOI 10.1002/app.47636.

11. Suwanamornlert, P., Kerddonfag, N., Sane, A., Chinsirikul, W., Zhou, W. et al. (2020). Poly(lactic acid)/poly (butylene-succinate-co-adipate) (PLA/PBSA) blend films containing thymol as alternative to synthetic

preservatives for active packaging of bread. *Food Packaging and Shelf Life, 25,* 100515. DOI 10.1016/j.fpsl.2020.100515.

12. Yu, Y. L., Xu, P. F., Jia, S. L., Pan, H. W., Zhang, H. L. et al. (2019). Exploring polylactide/poly(butylene adipate-co-terephthalate)/rare earth complexes biodegradable light conversion agricultural films. *International Journal of Biological Macromolecules, 127,* 210–221. DOI 10.1016/j.ijbiomac.2019.01.044.

13. Pivsa-Art, W., Pavasupree, S., O-Charoen, N., Insuan, U., Jailak, P. et al. (2011). Preparation of polymer blends between poly(L-lactic acid), poly(Butylene succinate-co-adipate) and poly(Butylene adipate-co-terephthalate) for blow film industrial application. *Energy Procedia, 9,* 581–588. DOI 10.1016/j.egypro.2011.09.068.

14. Nofar, M., Tabatabaei, A., Sojoudiasli, H., Park, C. B., Carreau, P. J. et al. (2017). Mechanical and bead foaming behavior of PLA-PBAT and PLA-PBSA blends with different morphologies. *European Polymer Journal, 90,* 231–244. DOI 10.1016/j.eurpolymj.2017.03.031.

15. Chen, W. W., Qi, C. Z., Li, Y., Tao, H. Y. (2021). The degradation investigation of biodegradable PLA/PBAT blend: Thermal stability, mechanical properties and PALS analysis. *Radiation Physics and Chemistry, 180,* 109239. DOI 10.1016/j.radphyschem.2020.109239.

16. Kopinke, F. D., Remmler, M., Mackenzie, K., Möder, M., Wachsen, O. (1996). Thermal decomposition of biodegradable polyesters—II. poly(lactic acid). *Polymer Degradation and Stability, 53(3),* 329–342. DOI 10.1016/0141-3910(96)00102-4.

17. Chen, B., Shen, C., Chen, S., Chen, A. F. (2010). Ductile PLA modified with methacryloyloxyalkyl isocyanate improves mechanical properties. *Polymer, 51(21),* 4667–4672. DOI 10.1016/j.polymer.2010.08.028.

18. Mansour, I. B., Alouani, K., Chauveau, E., Martin, V., Schiets, F. (2010). Synthesis and characterisation of poly (ester-amide)s from aromatic bisoxazoline precursors. *European Polymer Journal, 46(4),* 814–820. DOI 10.1016/j.eurpolymj.2009.12.014.

19. Xia, M. L., Shi, K. X., Zhou, M. Z., Shen, Y. C., Wang, T. W. (2019). Effects of chain extender and uniaxial stretching on the properties of PLA/PPC/mica composites. *Polymers for Advanced Technologies, 30(9),* 2436–2446. DOI 10.1002/pat.4691.

20. Najafi, N., Heuzey, M. C., Carreau, P. J., Wood-Adams, P. M. (2012). Control of thermal degradation of polylactide (PLA)-clay nanocomposites using chain extenders. *Polymer Degradation and Stability, 97(4),* 554–565. DOI 10.1016/j.polymdegradstab.2012.01.016.

21. Wang, X., Peng, S., Chen, H., Yu, X., Zhao, X. (2019). Mechanical properties, rheological behaviors, and phase morphologies of high-toughness PLA/PBAT blends by *in-situ* reactive compatibilization. *Composites Part B: Engineering, 173,* 107028. DOI 10.1016/j.compositesb.2019.107028.

22. Yan, Y., Dou, Q. (2021). Effect of peroxide on compatibility, microstructure, rheology, crystallization, and mechanical properties of PBS/Waxy starch composites. *Starch-Starke, 73(3–4),* 2000184. DOI 10.1002/star.202000184.

23. Ai, X., Li, X., Yu, Y. L., Pan, H. W., Yang, J. et al. (2019). The mechanical, thermal, rheological and morphological properties of PLA/PBAT blown films by using bis(tert-butyl dioxy isopropyl) benzene as crosslinking agent. *Polymer Engineering & Science, 59(S1),* E227–E236. DOI 10.1002/pen.24927.

24. Al-Itry, R., Lamnawar, K., Maazouz, A., Billon, N., Combeaud, C. (2015). Effect of the simultaneous biaxial stretching on the structural and mechanical properties of PLA, PBAT and their blends at rubbery state. *European Polymer JournaL, 68,* 288–301. DOI 10.1016/j.eurpolymj.2015.05.001.

25. Rzepna, M., Przybytniak, G., Sadło, J. (2018). Radiation degradation and stability of PBAT: Copolymer of aromatic and aliphatic esters. *Journal of Applied Polymer Science, 135(37),* 46682. DOI 10.1002/app.46682.

26. Gupta, A., Chudasama, B., Chang, B. P., Mekonnen, T. (2021). Robust and sustainable PBAT-Hemp residue biocomposites: Reactive extrusion compatibilization and fabrication. *Composites Science and Technology, 215,* 109014. DOI 10.1016/j.compscitech.2021.109014.

27. Baimark, Y., Srihanam, P. (2015). Influence of chain extender on thermal properties and melt flow index of stereocomplex PLA. *Polymer Testing, 45,* 52–57. DOI 10.1016/j.polymertesting.2015.04.017.

28. Arruda, L. C., Magaton, M., Bretas, R. E. S., Ueki, M. M. (2015). Influence of chain extender on mechanical, thermal and morphological properties of blown films of PLA/PBAT blends. *Polymer Testing, 43,* 27–37. DOI 10.1016/j.polymertesting.2015.02.005.

29. Li, X., Ai, X., Pan, H. W., Yang, J., Gao, G. H. et al. (2018). The morphological, mechanical, rheological, and thermal properties of PLA/PBAT blown films with chain extender. *Polymers for Advanced Technologies, 29(6),* 1706–1717. DOI 10.1002/pat.4274.

30. Gigante, V., Coltelli, M., Vannozzi, A., Panariello, L., Fusco, A. et al. (2019). Flat die extruded biocompatible poly (Lactic acid) (PLA)/Poly(Butylene succinate) (PBS) based films. *Polymers, 11(11),* 1857. DOI 10.3390/ polym11111857.

31. Ding, Y., Feng, W., Lu, B., Wang, P., Wang, G. (2018). PLA-PEG-PLA tri-block copolymers: Effective compatibilizers for promotion of the interfacial structure and mechanical properties of PLA/PBAT blends. *Polymer, 146,* 179–187. DOI 10.1016/j.polymer.2018.05.037.

32. Wang, X. Y., Weng, Y. X., Wang, W., Huang, Z. G., Wang, Y. Z. (2016). Modification of poly(propylene carbonate) with chain extender ADR-4368 to improve its thermal, barrier, and mechanical properties. *Polymer Testing, 54,* 301–307. DOI 10.1016/j.polymertesting.2016.07.024.

33. Al-Itry, R., Lamnawar, K., Maazouz, A. (2012). Improvement of thermal stability, rheological and mechanical properties of PLA, PBAT and their blends by reactive extrusion with functionalized epoxy. *Polymer Degradation and Stability, 97(10),* 1898–1914. DOI 10.1016/j.polymdegradstab.2012.06.028.

34. Al-Itry, R., Lamnawar, K., Maazouz, A. (2014). Reactive extrusion of PLA, PBAT with a multi-functional epoxide: Physico-chemical and rheological properties. *European Polymer Journal, 58,* 90–102. DOI 10.1016/j. eurpolymj.2014.06.013.

35. Nofar, M., Sacligil, D., Carreau, P. J., Kamal, M. R., Heuzey, M. (2019). Poly(lactic acid) blends: Processing, properties and applications. *International Journal of Biological Macromolecules, 125,* 307–360. DOI 10.1016/ j.ijbiomac.2018.12.002.

36. Bae, J. Y., Chung, D. J., An, J. H., Shin, D. H. (1999). Effect of the structure of chain extenders on the dynamic mechanical behaviour of polyurethane. *Journal of Materials Science, 34(11),* 2523–2527. DOI 10.1023/ A:1004680127857.

37. Spoljaric, S., Goh, T. K., Blencowe, A., Qiao, G. G., Shanks, R. A. (2011). Thermal, optical, and static/dynamic mechanical properties of linear-core crosslinked star polymer blends. *Macromolecular Chemistry and Physics, 212(16),* 1778–1790. DOI 10.1002/macp.201100143.

38. Abdelwahab, M. A., Taylor, S., Misra, M., Mohanty, A. K. (2015). Thermo-mechanical characterization of bioblends from polylactide and poly(butylene adipate-co-terephthalate) and lignin. *Macromolecular Materials and Engineering, 300(3),* 299–311. DOI 10.1002/mame.201400241.

39. Andrzejewski, J., Krawczak, A., Wesoły, K., Szostak, M. (2020). Rotational molding of biocomposites with addition of buckwheat husk filler. Structure-property correlation assessment for materials based on polyethylene (PE) and poly(lactic acid) PLA. *Composites Part B: Engineering, 202,* 108410. DOI 10.1016/j. compositesb.2020.108410.

40. Zhu, J., Zhao, X. Y., Liu, L., Yang, R. N., Song, M. et al. (2018). Thermodynamic analyses of the hydrogen bond dissociation reaction and their effects on damping and compatibility capacities of polar small molecule/nitrile-butadiene rubber systems, molecular simulation and experimental study. *Polymer, 155,* 152–167. DOI 10.1016/ j.polymer.2018.09.040.

41. Yang, C. X., Tang, H. B., Wang, Y. F., Liu, Y., Wang, J. et al. (2019). Development of PLA-PBSA based biodegradable active film and its application to salmon slices. *Food Packaging and Shelf Life, 22,* 100393. DOI 10.1016/j.fpsl.2019.100393.

42. Matos Costa, A. R., Crocitti, A., Hecker Carvalho, L., Carroccio, S. C., Cerruti, P. et al. (2020). Properties of biodegradable films based on poly(butylene succinate) (PBS) and poly(butylene adipate-co-terephthalate) (PBAT) blends. *Polymers, 12(10),* 2317. DOI 10.3390/polym12102317.